Reactivity of Stoichiometric and Defective TiO_2 (110) Surfaces toward DCOOD Decomposition

Qinggen Wang, Jurgen Biener, Xing-Cai Guo, Enrique Farfan-Arribas, and Robert J. Madix*

Department of Chemical Engineering and Chemistry, Stanford University, Stanford, California 94305

Received: April 29, 2003

The effect of defects on TiO_2 (110) on the decomposition of DCOOD was investigated by temperature-programmed reaction spectroscopy (TPRS). Different concentrations of anion vacancy defects were created on the TiO_2 (110) surface by electron beam irradiation in order to minimize structural damage to the surface. For comparison, defects were also created by argon bombardment. The oxidation state produced by the defects and their concentrations were characterized by X-ray photoelectron spectroscopy (XPS). The selectivity of the reaction for the production of carbon monoxide, formaldehyde, and D_2 was increased significantly by the defects. An appreciable decrease in the temperature for CO and D_2CO formation on the defective surfaces produced by electron beam irradiation was observed, compared to the stoichiometric surface, suggestive of changes in the kinetics of the decomposition. The presence of isotopic exchange in the products provides evidence for the formation of formyl intermediates during DCOOD decomposition.

I. Introduction

TiO_2 is widely used as a catalyst support in industry and as a photocatalyst for water dissociation. Its surface structure and reactivity have been studied extensively in recent years utilizing single crystals.[1−17] Among the low-index single-crystal surfaces, the (110) face is the most stable, and it has received considerable attention in the surface science literature. The TiO_2 (110) surface exposes rows of coordinatively unsaturated titanium cations, which, along with neighboring oxygen anions, form potential Lewis acid−base pairs. The Lewis acid sites can bond electron-donor molecules and/or act as coordination sites for the conjugate base of an acidic reactant, such as formic acid. Indeed, formate ions have been shown by scanning tunneling microscopy to coordinate to these cations, forming highly ordered structures along the [001] direction.[3]

Point defects on surfaces are believed to play an important role in catalysis.[18] For example, on TiO_2 (110) defects are required for water dissociation, and they also lead directly to the reduction of formaldehyde.[19] The most common methods used to create defects on TiO_2 surfaces are high-temperature annealing, electron-beam irradiation, and argon-ion bombardment.[19−26] On the TiO_2 (110) surface, high-temperature annealing produces a variety of surface structures due to the migration of titanium cations to the surface,[27] and argon bombardment creates substantial disruption of the surface order.[3] We have chosen electron irradiation for defect generation because it is expected to generate anion vacancy defects, generating less structural disorder, at least at low defect concentration.[28]

Several studies of the effects of defects on TiO_2 surfaces, generated by different methods, on the adsorption and/or reaction of small molecules have been reported in the literature.[19,23,24,26,29−36] Generally, these studies show two effects: (1) oxygen vacancy defects can cause reduction (e.g., water, NO, and CH_2O) or dehydration (e.g., alcohols); (2) high degrees of coordinative unsaturation of the titanium cations can lead to coupling reactions, presumably via multiple coordination of reactants to the same cation, as suggested by Kim and Barteau.[26]

Formic acid decomposition has been studied on stoichiometric TiO_2 (110) surfaces;[37,38] formaldehyde was observed in one case and the production of formaldehyde was proposed to be related to oxygen vacancies on the surface.[38] In this work the effects of defects created by both electron-beam irradiation and argon-ion bombardment on the kinetics of the decomposition of formic acid have been studied further by controlling the defect concentration. A reasonable mechanism to explain their effects, which involves the participation of formyl as an intermediate in the formation of both CO and formaldehyde, is formulated. Furthermore, important differences in the effects of Ti^{3+} defects introduced by ion bombardment and electron irradiation are noted.

II. Experimental Section

The experiments were performed in a UHV system that consists of adjoined preparation and spectroscopy chambers. The preparation chamber is equipped with a sputter-ion gun and gas dosers. The spectroscopy chamber is equipped with LEED optics, a Perkin-Elmer 04-548 dual anode X-ray source, an EA 10 Plus hemispherical energy analyzer from SPECS, a UTI 100c quadrupole mass spectrometer, and a syringe-needle gas doser. The base pressures of the preparation chamber and the spectroscopy chamber were 6×10^{-10} Torr and 3×10^{-10} Torr, respectively. During the XPS and TPRS measurements the preparation chamber was isolated from the spectroscopy chamber.

The polished TiO_2 (110) rutile single crystal ($10 \times 10 \times 1$ mm^3, supplied by Atomergic Chemetals, Corp.) was supported by a tantalum foil. The foil was resistively heated via two tantalum wires spot-welded to the back of the foil, and the crystal was heated by conduction. The temperature was monitored by a Chromel-Alumel thermocouple glued to the side of the crystal with ceramic adhesive (Aremco Products, Inc.). After cycles of sputtering and annealing, the crystal appeared light

* Corresponding author. E-mail: rjm@chemeng.stanford.edu.

10.1021/jp030511i CCC: $25.00
Published on Web 09/27/2003

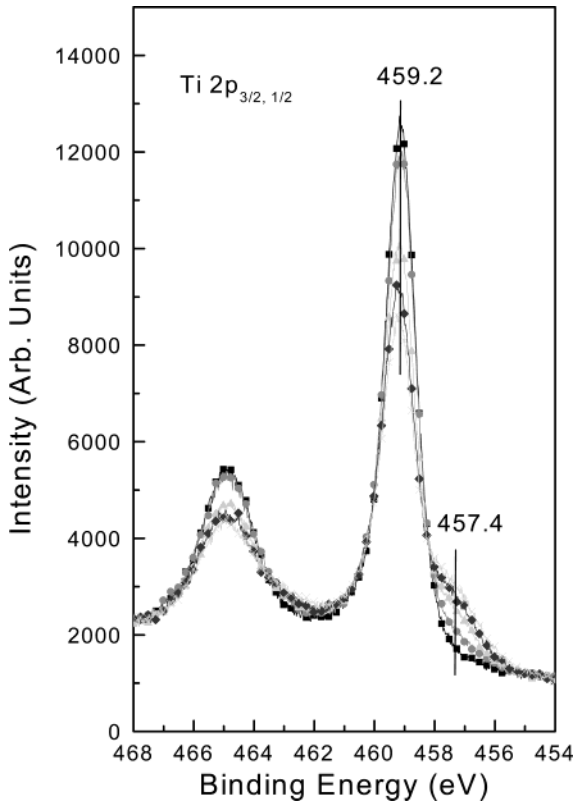

Figure 1. Ti 2p core-level XP spectra of TiO_2 (110) surfaces: stoichiometric surface (■), surfaces irradiated by electron beam for 5 min (●), 7 min (▲), 10 min (◆), and 15 min (x).

blue. Before each experiment the TiO_2 (110) surface was cleaned by sputtering for 30 min with 500 eV argon ions, followed by annealing in a vacuum at 850 K for 15 min.

Defects were created both by irradiation with electrons and by argon-ion bombardment. For electron irradiation the crystal surface was biased at 300 V and exposed to electrons emitted from a nearby hot filament. Currents measured were typically 0.7 mA, but as the sample holder was also exposed to the electron beam, the estimated current on the sample is about one-tenth of that measured. Argon ions were generated by a conventional sputtering gun (Physical Electronics) with 5×10^{-5} Torr argon and 500 eV high voltage, the current density at the sample was $\sim 6\ \mu A/cm^2$.

The cleanliness and composition of the surface were checked by XPS using nonmonochromatic Mg Kα X-rays. The photoelectrons emitted normal to the sample surface were collected by the energy analyzer at a pass energy of 25 eV. Binding energies were calibrated by the Au 4f peak (84.00 eV). DCOOD (Aldrich, 99+ atom % D) was used for temperature-programmed reaction studies. DCOOD liquid was outgassed by freeze−pump−thaw cycles before use each day. In each TPRS experiment, identical saturation DCOOD doses were administered through the needle doser at room temperature. TPR spectra were recorded by a computer coupled with the mass spectrometer, whose ionizer was enclosed in a glass cap with a small hole facing the crystal surface.

III. Results

A. Surface Characterization. The surface composition was first characterized by XPS (Figure 1). In the absence of Ar^+ bombardment or electron-beam irradiation there existed only one symmetric Ti $2p_{3/2}$ peak centered at 459.2 eV, consistent with the binding energies reported for Ti^{4+} $2p_{3/2}$ on rutile (110) surfaces.[24,39,40] Hence the surface prepared was assumed to be stoichiometric, though the existence of a small concentration of anion defects is possible.

TABLE 1: Surface Composition of TiO_2 (110) As Characterized from Ti $2p_{3/2}$ XPS Peak on Surfaces of Different Exposure Times to Electron Irradiation at 300 eV and Ar Bombardment for 1 min

	TiO_2	E5	E7	E10	E15	Ar1
Ti^{4+} percentage	100%	97%	90%	85%	81%	81%
Ti^{3+} percentage	0%	3%	10%	15%	19%	19%
oxygen defect concentration (ML)	0	0.06	0.21	0.32	0.40	0.40

Electron-beam irradiation introduces defects to the surface. It is believed that the defects produced are anion vacancy defects produced by electron-stimulated desorption (ESD) of surface-bridging oxygen ions, though desorption of in-plane oxygen ions cannot be ruled out completely. Further, at least at low concentration of defects, the overall surface structure is relatively undamaged during the process.[20,28] For the exposure times studied here, only Ti^{3+} defects were produced on the surface, as indicated by the additional Ti $2p_{3/2}$ peak centered at 457.4 eV in Figure 1. It was also observed on other surfaces that the Ti^{3+} $2p_{3/2}$ peak had a binding energy ~1.8 eV lower that that of Ti^{4+} $2p_{3/2}$ peak.[21,41]

By varying the exposure time, surfaces with a wide range of defect concentrations were prepared. The area of the Ti^{3+} $2p_{3/2}$ peak increased from 0 to 19% of the total area of the Ti $2p_{3/2}$ peaks as the exposure to the electrons was increased. The percentage areas of Ti^{3+} and Ti^{4+} $2p_{3/2}$ peaks for the surfaces prepared in this manner are listed in Table 1. For simplicity, in this paper the stoichiometric surface is designated as TiO_2, the surface irradiated by electron beam for 5 min as E5, and the surface bombarded by Ar^+ for 1 min as Ar1. Other surfaces were designated in analogous fashion. Table 1 also lists the estimated defect concentration at the surface. The concentration was estimated using the published value for the escape depth of electrons from the TiO_2 (110) surface,[39] assuming that Ti^{3+} cations reside only on the top layer. In this way the defect concentration following 15 min of irradiation by electrons is estimated to be approximately 40% of a monolayer (1 monolayer $= \sim 1.04 \times 10^{15}$ sites cm^{-2}). For the surface of such high defect density we may anticipate some surface reconstruction to occur to accommodate the high polarity on the surface due to the existence of Ti^{3+}. Extensive reconstruction is not likely as the (1×1) LEED pattern is still discernible on such surface, though with a high background (see below).

Argon-ion bombardment creates Ti^{3+} point defects through preferential sputtering of oxygen ions. After Ar^+ bombardment, only Ti^{3+} defects were detected by XPS; the Ti^{3+} $2p_{3/2}$ peak was slightly sharper than those observed on electron-irradiated surfaces. The Ti^{3+} $2p_{3/2}$ peak area was 16% of the total area of the Ti $2P_{3/2}$ peaks after 1 min sputtering—a concentration close to that observed for the E15 surface. The XPS spectrum of the Ar^+ sputtered surface is shown in Figure 2 as an illustration of the peaks used for peak fitting for the Ti XP spectra obtained in this set of experiments. Scanning tunneling microscopy reveals that Ar^+ bombardment severely disrupts the surface structure. The bombarded surface is much rougher than the original surface; small islands ca. 4 nm in diameter are formed, and long-range order is severely reduced.[3]

The structure of these surfaces was also studied by LEED. The images are shown in Figure 3. The stoichiometric surface gave a sharp 1×1 pattern. When the surface was subjected to electron irradiation, the LEED spots became more diffuse, and the background became brighter with longer irradiation time.

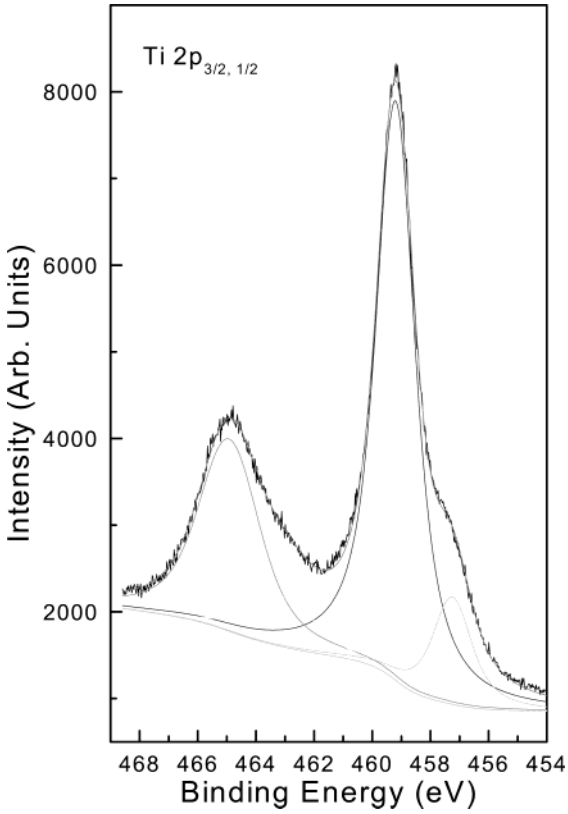

Figure 2. Peak fitting of Ti 2p core-level XP spectrum of TiO_2 (110) surface bombarded by Ar^+ for 1 min.

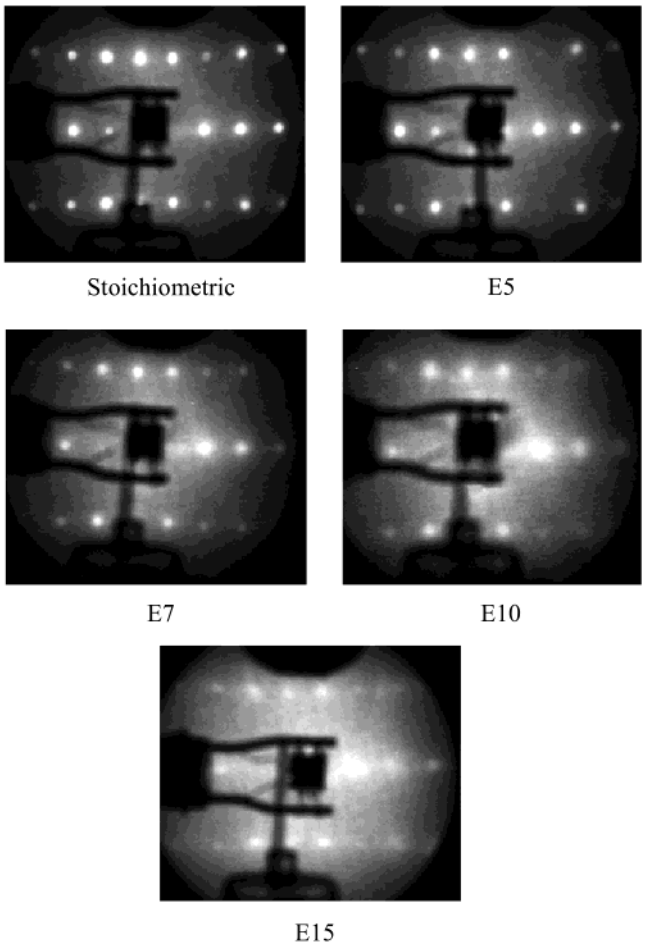

Figure 3. LEED pattern observed on stoichiometric surface, surfaces irradiated by electron beam for 5, 7, 10, and 15 min.

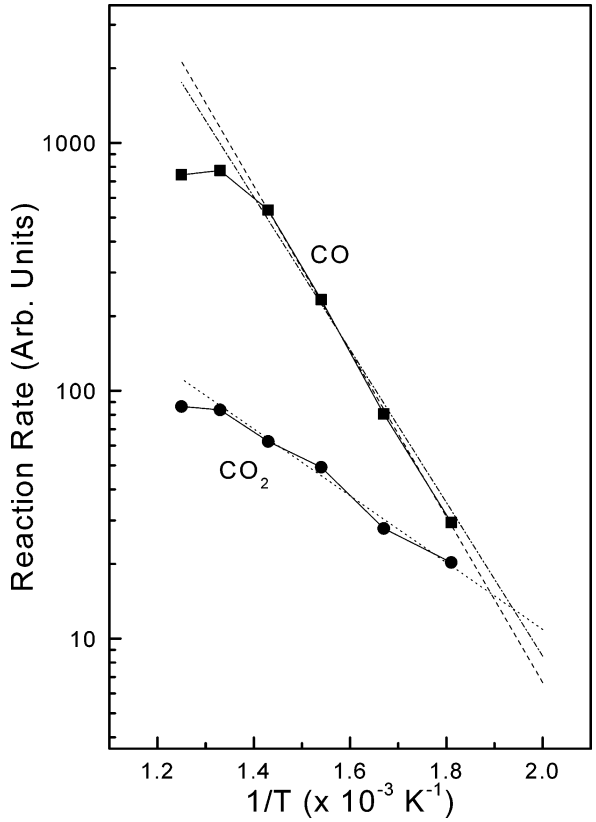

Figure 4. Rates of the products in steady-state DCOOD decomposition: CO (■) and CO_2 (●). Dashed line is the fitting for CO reaction, dotted line for CO_2 reaction. ·-· line is the fitting using the activation energy determined by Henderson.[38]

But even after electron irradiation for 15 min, the 1×1 LEED pattern persisted. For the surface sputtered with Ar^+ for 1 min, no LEED pattern could be detected. The LEED results confirm that the TiO_2 (110) surface was not disrupted by electron radiation significantly, while Ar^+ sputtering destroyed the long-range structure on the surface completely.[3]

B. Steady-State Reaction on a Stoichiometric Surface. For reference we first examined the steady-state catalytic activity of stoichiometric TiO_2 (110) for the DCOOD decomposition in a fashion similar to that conducted by Onishi et al.[37] and Bowker et al.[9] The pressure of formic acid used was 2×10^{-7} Torr. Our results closely paralleled the results of Onishi et al. Two channels for DCOOD decomposition to CO and CO_2 were observed, and the decomposition of DCOOD to CO has a higher activation energy than that for CO_2 formation. The effect of temperature on the parallel reaction routes to CO and CO_2 is plotted in Figure 4. By extrapolating the fit of the experimental data, the crossover in reactivity to form CO or CO_2 was estimated to be 525 K; this result is qualitatively in agreement with Onishi et al. who reported that the rate of the dehydrogenation reaction exceeded that of the dehydration reaction below 500 K. The activation energies deduced for CO and CO_2 formation are 63.5 kJ mol^{-1} and 27 kJ mol^{-1}, respectively. For comparison, a dot−dash−dot line is drawn through our data for CO using the activation energy determined by Henderson.[38] The agreement is quite good. In contrast, Bowker et al.[9] did not observe the dehydrogenation reaction in their molecular beam experiments. The origin of this difference is unknown. Since the surface must be "conditioned" in the beam for a period of time before steady-state is reached, there may be subtle differences in surface structure among the three studies that influence reactivity.

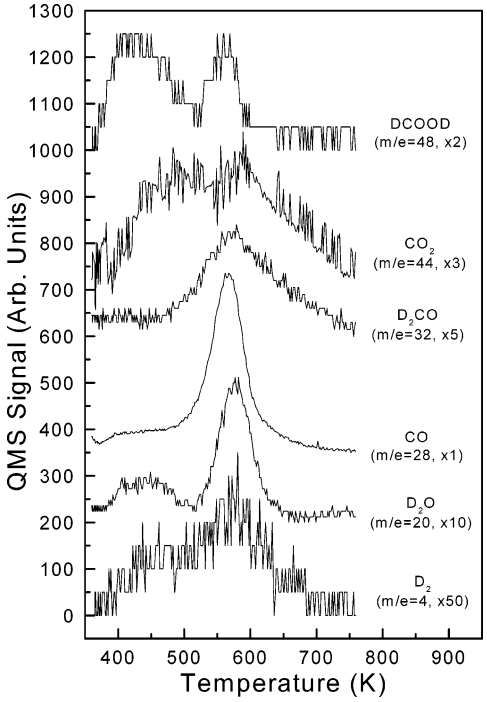

Figure 5. TPR spectra for saturation exposure of DCOOD on stoichiometric TiO_2 (110) at room temperature. The signals are corrected by QMS sensitivity.

C. TPRS on Stoichiometric and Defective Surfaces. In agreement with previous work,[38] we observed DCOOD to decompose into CO, D_2CO, CO_2, D_2O, and D_2 on both the stoichiometric and defective TiO_2 (110) surfaces. Methanol was not observed. The TPR spectrum for DCOOD decomposition on the stoichiometric surface following the adsorption of formic acid near room temperature is shown in Figure 5. The CO_2 spectrum was corrected by subtracting the cracking fraction from DCOOD. Among the decomposition products, CO and D_2O were the major products (~60%), D_2CO and CO_2 were minor products (~10%), and a small amount of D_2 (~2%) was observed as well.

The effects of defects on the formation of each of the different products are now described separately. General discussion of the implications of the effects of the defects then follows in the Discussion section.

(i) CO. Figure 6 shows CO/DCOOD TPR spectra for each surface. The peak temperatures for CO, as well as for other products, on each surface studied are listed in Table 2. CO was evolved at 566 K in a single peak on the stoichiometric surface. The peak shape and peak temperature resemble those reported by Henderson.[38] Assuming a preexponential factor of 2×10^9 s^{-1},[37] the activation energy for the formation of gaseous CO was estimated from the TPR spectrum to be 112 kJ mol^{-1} for the stoichiometric surface, which is in good agreement with the result of Onishi et al. (120 kJ mol^{-1}).[37]

After the stoichiometric surface was irradiated with the electron beam, an additional CO peak appeared around 465 K. This peak is broader than the peak on the stoichiometric surface, and its intensity increases with the irradiation time. The low-temperature channel becomes the dominant one on E10, and on E15 most of the CO originates from this low-temperature channel. The area percentage of the CO produced from each channel on the different surfaces is listed in Table 3. The area was calculated by fitting each spectrum with two Gaussian peaks; a sample fit is shown in Figure 6 for the E10 surface. It

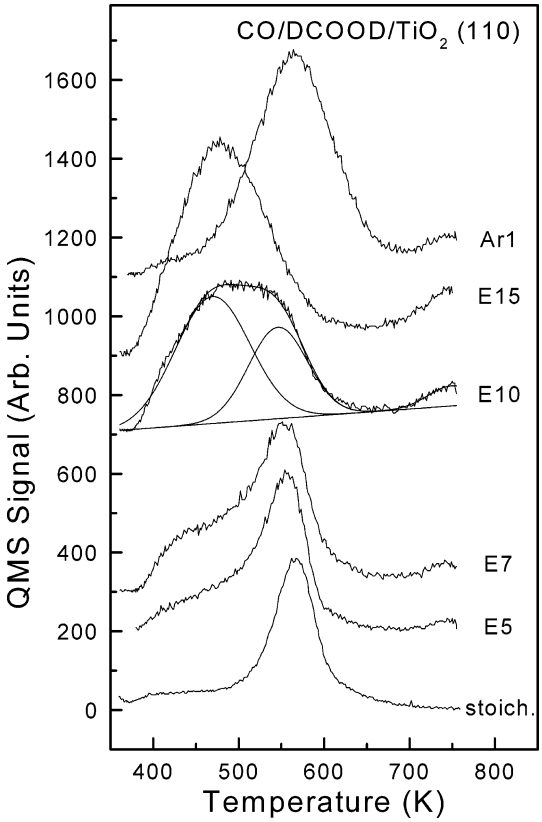

Figure 6. CO TPRS spectra from DCOOD decomposition on TiO_2 (110) surfaces: stoichiometric surface, surfaces irradiated by electron beam for 5 min, 7 min, 10 min, 15 min, and surface bombarded by Ar^+ for 1 min.

TABLE 2: Peak Temperature of the Products from DCOOD TPRS on the Surfaces Studied

	D_2 (K)		D_2O (K)		CO (K)		D_2CO(K)	CO_2 (K)		DCOOD(K)	
TiO_2	444	575	438	577	–	567	575	475	585	411	564
E5	427	560	438	579	462	555	528	456	580	410	554
E7	436	566	410	583	466	553	487	476	577	417	562
E10	428	535	404	575	470	546	479	456	590	408	543
E15	428	517	408	538	474	541	472	496	580	410	508
Ar1	428	591	410	606	–	567	556	436	613	410	564

TABLE 3: Area Percentage of CO from Low- and High-Temperature Channels on Electron-Irradiated Surfaces

	TiO_2	E5	E7	E10	E15
low temp	0%	33%	42%	66%	83%
high temp	100%	67%	58%	34%	17%

is obvious from Figure 6 that the area of the high-temperature CO peak shrinks with the irradiation time. This implies that the high-temperature channel is short-circuited by the existence of the low-temperature channel. CO desorption from the CO-dosed E10 surface occurred at 425 and 465 K, suggesting that CO evolution at 560 K from the electron-irradiated surfaces is reaction limited in the case of formic acid.

The existence of two CO desorption channels may be related to the adsorption configuration of formate on a defective surface. On the stoichiometric surface one formate occupies two neighboring 5-fold coordinated Ti^{4+} cations (Figure 7, configuration A, α-bridging).[42−44] Recent studies by HREELS, STM, and NC-AFM have confirmed the bidentate nature of this formate species, in good agreement with theoretical calculations.[11,15−17] On a defective surface a formate may take other

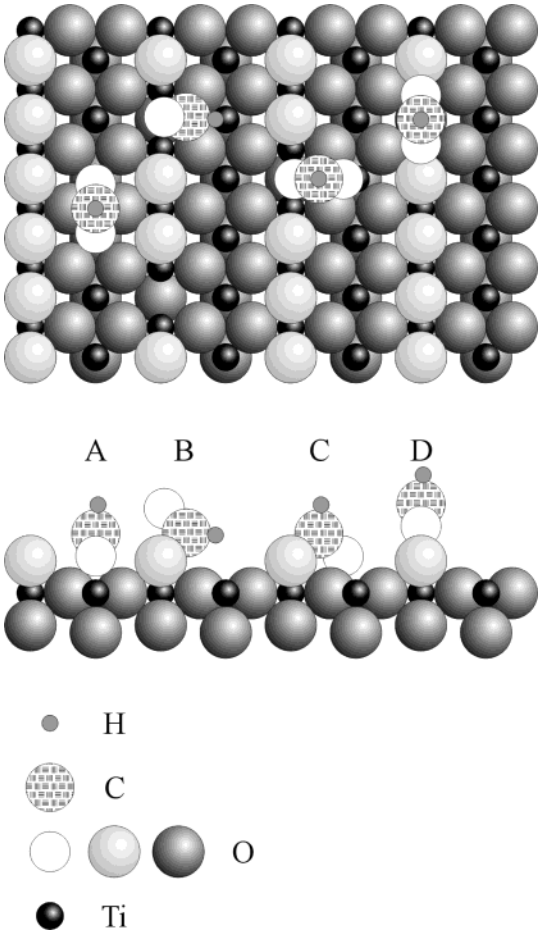

Figure 7. Schematic representations of the various configurations for formate on an electron-irradiated TiO_2 (110) surface.

configurations. The possible adsorption geometries of formates on a defective surface with oxygen vacancies in the bridging oxygen rows are shown in Figure 7. Among the configurations, one of the oxygen atoms in a formate may occupy one oxygen vacancy (coordinating with two Ti^{3+} sites) in the bridging oxygen row, while the other oxygen atom either dangles (configuration B, monodentate) or bonds with a Ti^{4+} site in the neighboring row (configuration C, β-bridging). A formate can also take configuration D in which it bonds to two neighboring Ti^{3+} sites which originated from one oxygen vacancy. Configuration D is similar to A, but it is presumably less stable since one oxygen vacancy may not provide enough space to accommodate the two oxygen atoms of the formate. The existence of two neighboring oxygen vacancies in the bridging oxygen row of significant concentration was excluded by the fact that no Ti^{2+} was detected by XPS. Likely the most stable form is β-bridging, as it has been suggested by theoretical calculations[24] and detected by absorption IR spectroscopy on the TiO_2 (110) surface.[45] Different studies using HREELS,[15] NEXAFS,[14] and STM[9] have provided additional evidence of the existence of a second formate species. Monodentate and β-bridging configurations will reduce the number of pairing Ti^{4+} sites available for formate adsorption in α-bridging configuration, hence less CO would appear in the high-temperature peak. The generation of oxygen vacancies in the in-plane oxygen rows may be another source of the reduction of the amount of formate in α-bridging configuration; however, the number of such oxygen vacancies is expected to be insignificant.[20,28] Using the same preexponential factor for CO production on the stoichiometric surface, we estimated an activation energy of 92 kJ mol^{-1} for the low-temperature channel—30 kJ mol^{-1} lower than the high-temperature channel. Defects introduced by electron-beam irradiation are much more active at decomposing DCOOD to CO than the 5-fold coordinated Ti^{4+} sites exposed on the stoichiometric TiO_2 (110) surface.

TABLE 4: Selectivity to CO, D_2CO, and CO_2 of DCOOD Decomposition on Different Surfaces

	TiO_2	E5	E7	E10	E15	Ar1
CO	58%	63%	67%	62%	65%	73%
D_2CO	10%	20%	22%	34%	32%	22%
CO_2	32%	16%	11%	5%	3%	5%

However, compared to the stoichiometric surface, the CO desorption peak on the defective surface created by argon bombardment did not move, but broadened and exhibited an increase in peak area. Therefore the defects introduced by Ar^+ bombardment increased the selectivity toward CO but not the reactivity. Considering that the extent of reduction on the Ar1 surface is similar to that on the E15 surface, this shows that DCOOD decomposes more easily in the presence of anion vacancy defects in the regular TiO_2 (110) structure; i.e., on the surface after electron exposure. The local environment of the defects clearly plays a significant role in determining the reactivity. That the reactivity of DCOOD decomposition to CO is sensitive to the structure of the substrate surface can also be exemplified by comparing reactions on TiO_2 (110) and TiO_2 (100) surfaces.[38,46] It has been shown that, under similar experimental conditions, formic acid decomposed to CO on the stoichiometric TiO_2 (100) (1×1) surface at 590 K, while on the TiO_2 (110) (1×1) surface it decomposed at ~560 K. Finally, the difference observed between the effects of the argon bombardment and electron irradiation make it clear that the structures of the two resulting surfaces differ appreciably.

CO remains the dominant decomposition product on all surfaces studied, as illustrated by the selectivity to CO listed in Table 4. When calculating the selectivity, it was assumed that CO, D_2CO, and CO_2 were the only carbon-containing decomposition products, and both channels of the CO formation were taken into account. The signals were corrected for the mass spectrometer sensitivity. Table 4 also shows that the overall selectivity to CO did not vary much on the defective surfaces produced by electron irradiation.

(ii) D_2O. By stoichiometry the formation of CO would be expected to lead to similar amounts of water. Overall, however, the amount of D_2O formed decreases with electron irradiation time, which is consistent with oxygen being used to fill the oxygen vacancies. The D_2O TPRS peaks from the different surfaces are shown in Figure 8. In contrast to the results for CO, on the stoichiometric surface D_2O is formed in two separate reaction channels; one occurs at 440 K, and the other occurs at 577 K, neither of which corresponds to the temperature of CO formation. These two channels are observed on all electron-irradiated surfaces, with the high-temperature peak changing from the major to the minor feature as irradiation time increases. Interestingly, the temperature of these two peaks on all the surfaces shows little shift, except that the high-temperature peak on the E15 surface was about 40 K lower than on all the other electron-irradiated surfaces.

On the Ar^+-bombarded surface both the low- and the high-temperature features are reduced to a similar magnitude, but the high-temperature peak is much wider than the low-temperature one. Compared with the stoichiometric surface, the peak temperature of the low-temperature channel shifts to lower temperature and becomes sharper, while the second peak shifts to a higher temperature.

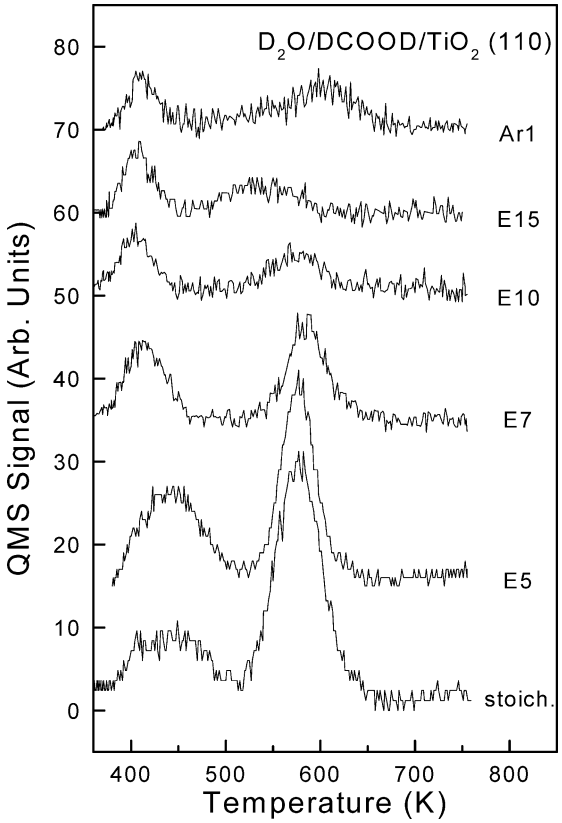

Figure 8. D_2O TPRS spectra from DCOOD decomposition on TiO_2 (110) surfaces: stoichiometric surface, surfaces irradiated by electron beam for 5 min, 7 min, 10 min, 15 min, and surface bombarded by Ar^+ for 1 min.

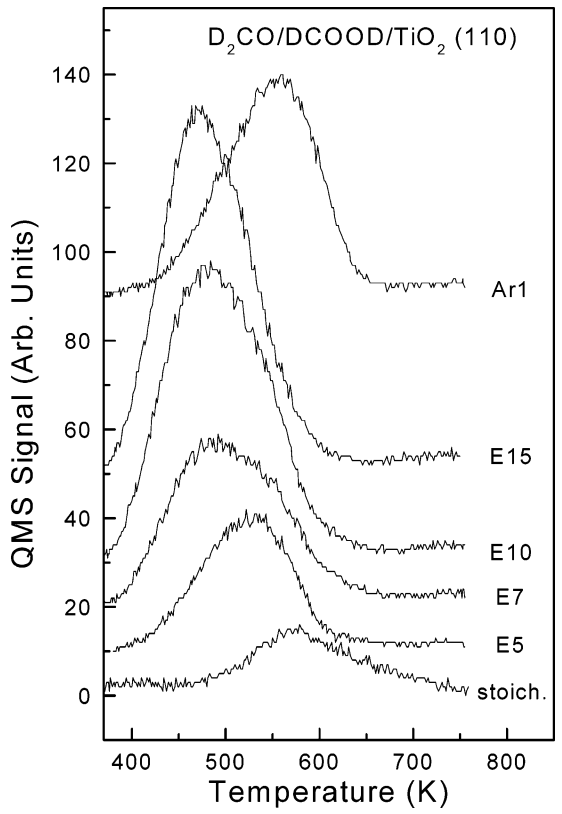

Figure 9. D_2CO TPRS spectra from DCOOD decomposition on TiO_2 (110) surfaces: stoichiometric surface, surfaces irradiated by electron beam for 5 min, 7 min, 10 min, 15 min, and surface bombarded by Ar^+ for 1 min.

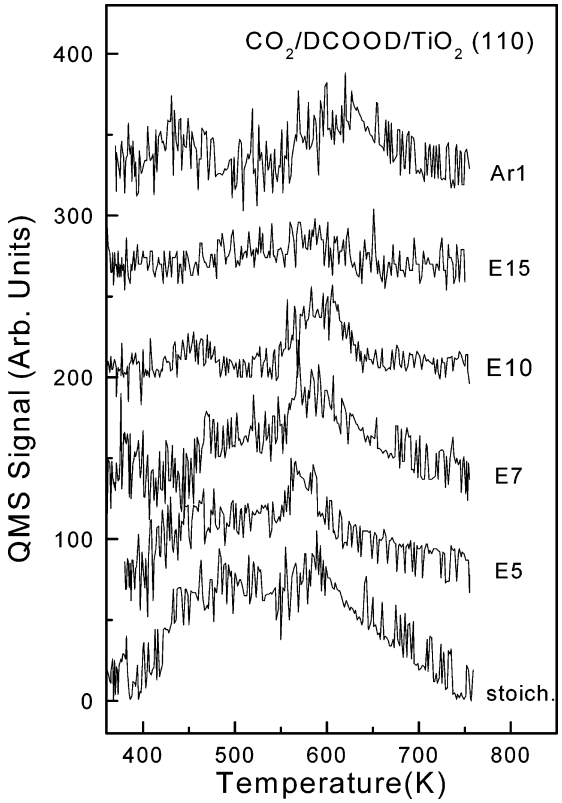

Figure 10. CO_2 TPRS spectra from DCOOD decomposition on TiO_2 (110) surfaces: stoichiometric surface, surfaces irradiated by electron beam for 5 min, 7 min, 10 min, 15 min, and surface bombarded by Ar^+ for 1 min.

(iii) D_2CO. The D_2CO TPRS from all surfaces studied is shown in Figure 9. On the stoichiometric surface the peak temperature was only slightly higher than that of CO (Table 2). With the increase of the electron irradiation time, the D_2CO peak shifted steadily to lower temperature, from 575 K on the stoichiometric surface to 471 K on the E15 surface. On all these surfaces the peak temperature for D_2CO formation was significantly lower than that for CO evolution in the higher temperature channel. The selectivity for D_2CO increased with defect concentration, from 10% on the stoichiometric surface to 34% on the surface irradiated by electrons for 10 min (Table 4). On the Ar^+-bombarded surface the D_2CO peak temperature was only slightly lower than that for CO. The selectivity to D_2CO was higher than the stoichiometric surface, lower than the E15 surface, and similar to the E7 surface. The increase in D_2CO production appears to be at the expense of CO_2 formation.

(iv) CO_2. Figure 10 shows the CO_2 product spectra, corrected for the cracking fraction of DCOOD. On the stoichiometric surface the CO_2 spectrum shows peaks at 475 and 585 K, with both peaks showing similar intensity. The area of both peaks decreases as the electron irradiation time increases, but the low-temperature peak decreases faster, and it almost disappears on the surface irradiated for 15 min. The presence of defects created by electron beam suppressed the decomposition of formate to CO_2. For the electron-irradiated surfaces there are variations in the temperature of both the high- and low-temperature peaks, but variations appear to be small.

When the surface was bombarded with Ar^+, the amount of CO_2 decreased in both the low- and high-temperature range. The low-temperature peak shifted to lower temperature, while the high-temperature peak shifted to higher temperature. This behavior differs sharply from that observed on the electron-beam-irradiated surfaces.

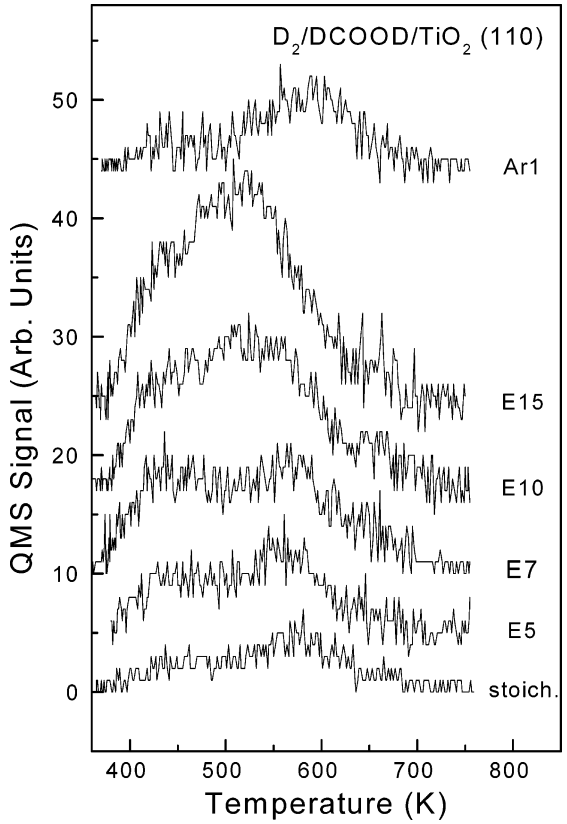

Figure 11. D_2 TPRS spectra from DCOOD decomposition on TiO_2 (110) surfaces: stoichiometric surface, surfaces irradiated by electron beam for 5 min, 7 min, 10 min, 15 min, and surface bombarded by Ar^+ for 1 min.

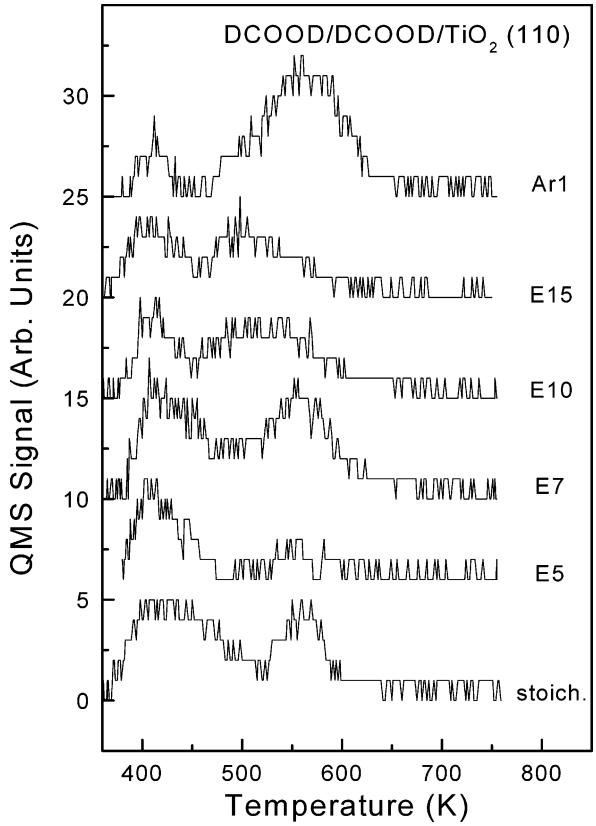

Figure 12. DCOOD TPRS spectra from DCOOD decomposition on TiO_2 (110) surfaces: stoichiometric surface, surfaces irradiated by electron beam for 5 min, 7 min, 10 min, 15 min, and surface bombarded by Ar^+ for 1 min.

(v) D_2. Figure 11 shows the TPR spectra of D_2 for the different surfaces. On the stoichiometric surface D_2 desorbed at 440 and 573 K. The low-temperature peak was smaller in intensity than the high-temperature one. After the surface was irradiated by electrons, both the low- and high-temperature peaks increased in magnitude with the defect concentration, and the high-temperature peak shifted slightly to lower temperature. On the Ar^+-bombarded surface the two-peak feature still remained, but the high-temperature peak had a higher intensity and shifted to higher temperature compared with the stoichiometric surface, the low-temperature peak had almost no change. The amount of D_2 desorbed was significantly less than that on the E15 surface, which had a Ti^{3+} concentration similar to the Ar^+-bombarded surface.

(vi) DCOOD. The amount of DCOOD desorbed from the stoichiometric surface is small, though peaks with similar intensities are discernible at 406 and 566 K (Figure 12). These features have previously been assigned to reaction of formate and hydroxyl species.[38] After defects were introduced by electron irradiation, the DCOOD formation appeared to be slightly suppressed at the low-temperature peak, and there is no obvious trend in the change of the high-temperature peak. After Ar^+ bombardment, neither peak shifts, but the low-temperature peak shrinks and the other peak shows a large increase in intensity.

D. Isotopic Effects. A mixture of $H^{13}COOH$ and DCOOH was dosed onto the stoichiometric and the E15 surfaces. Peaks for CO ($m/e = 28$) and ^{13}CO ($m/e = 29$) are shown in Figure 13. On both surfaces the ^{13}CO peak leads the CO peak by about 8 K. On the stoichiometric surface the ^{13}CO and CO peaks show similar intensity, while on the E15 surface, the CO peak is about 30% higher than the ^{13}CO peak.

HCOOD was used as a reagent on the E10 surface to ascertain whether the H−C bond breaks when forming formaldehyde. No D_2CO ($m/e = 32$) was detected in this experiment, revealing that intermediates necessitating cleavage of the H−C bond are not involved in formaldehyde formation.

E. Oxidizability of the Defective Surfaces. The left panel of Figure 14 shows the Ti 2p X-ray photoelectron spectra of the E15 surface after being dosed with DCOOD at room temperature and subsequently flashed to 450 and 600 K in less than 1 min. The spectra were taken at room temperature. It took about 5 min for the sample to cool from 600 K to room temperature. As the figure shows, even at room temperature the DCOOD reoxidized the defects to a small extent. The surface was oxidized further after the sample was flashed to 450 K, at which temperature formate started decomposing. At this point about half of the Ti^{3+} was oxidized to Ti^{4+}. Most of the Ti^{3+} (~80%) was oxidized to Ti^{4+} at 600 K, at which temperature most of the formate on the surface has decomposed. For the Ar^+-bombarded surface the oxidation was noticeable (~20%, Figure 14, right) only after the DCOOD-dosed surface was flashed to 600 K. Most of the formate on the surface has decomposed at this temperature. The oxidation of the surface defects was mainly due to the presence of formate, the diffusion of Ti^{3+} from the surface to the bulk did not play a major role. Without DCOOD adsorption, no oxidation was detectable of the Ar1 surface after it was flashed to 600 K. Only about 35% Ti^{3+} was oxidized to Ti^{4+} on the E15 surface under the same conditions, while no oxidation was observed after the surface was flashed to 450 K. The difference between the oxidizability of the electron irradiated and the Ar^+-bombarded surfaces again suggests that the defect structures of Ti^{3+} cations on these surfaces are not the same.

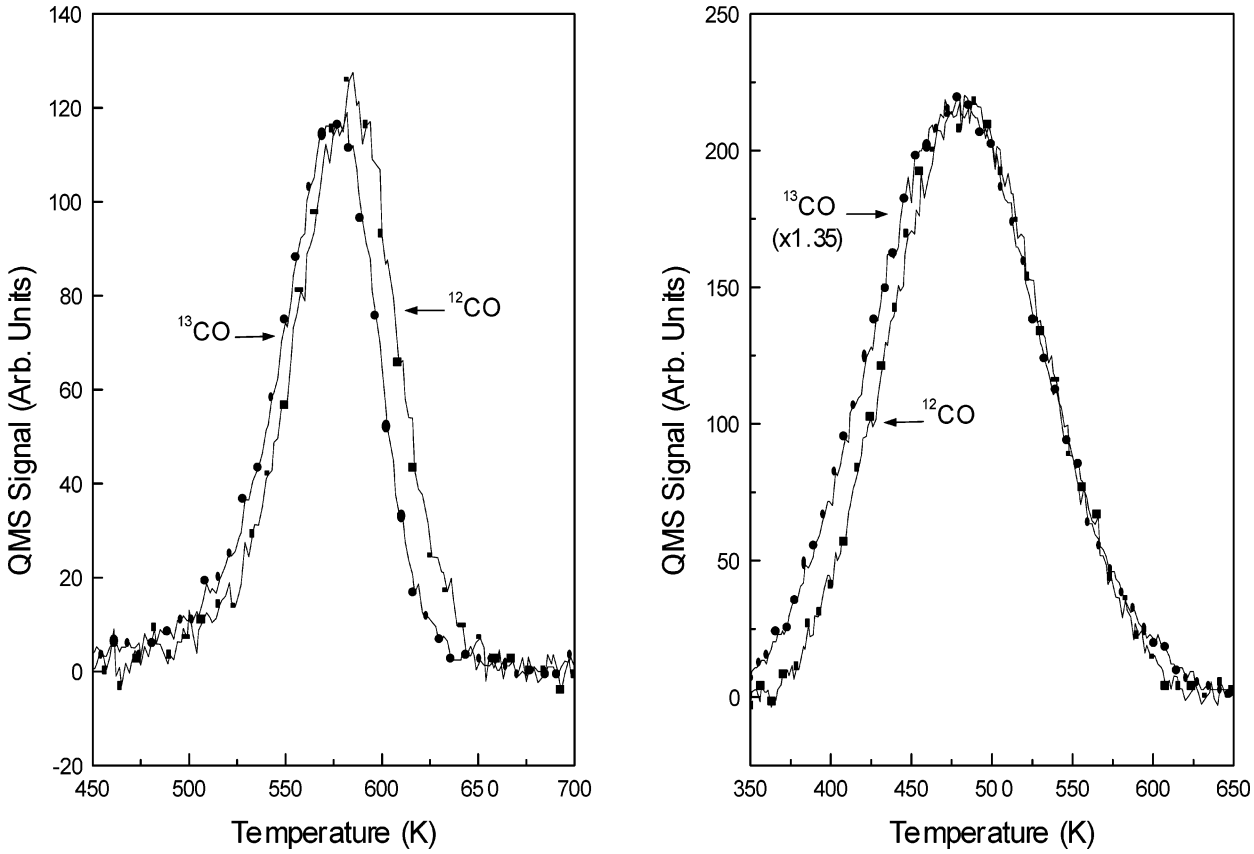

Figure 13. ^{12}CO (■) and ^{13}CO (●) TPRS spectra from a mixture of D^{12}COOH and H^{13}COOH decomposition on stoichiometric TiO_2 (110) surface (left) and TiO_2 (110) surface irradiated by electron for 15 min (right).

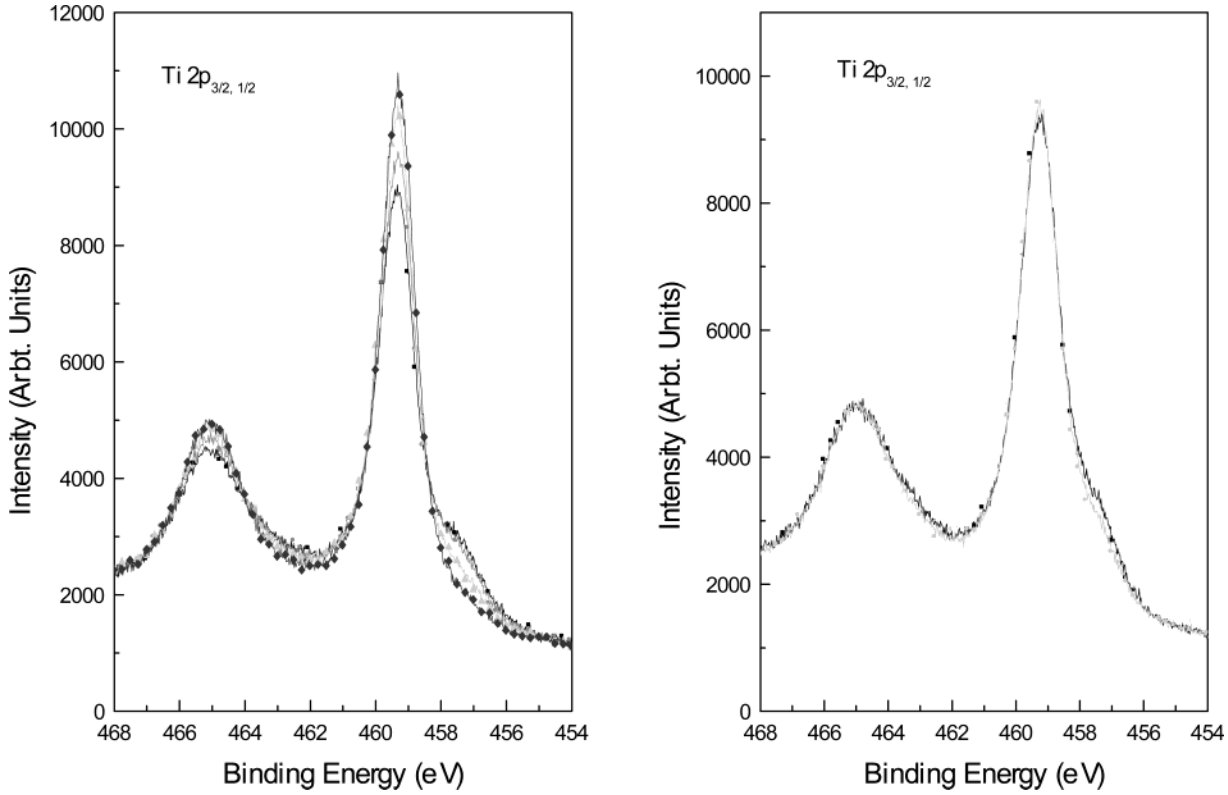

Figure 14. Left: Ti 2p core-level XPS spectra of TiO_2 (110) surfaces irradiated for 15 min (■), after dosing DCOOD (●) at room temperature followed by flashing to 450 K (▲) and 600 K (◆). Right: Ti 2p core-level XPS spectra of TiO_2 (110) surfaces bombarded by Ar^+ for 1 min (■), after dosing DCOOD at room temperature followed by flashing to 600 K (●).

The influence of anion vacancy defects on the decomposition of the formate was explored with oxygen post-dosing experiments. The experiments consisted in adsorbing HCOOH on the E10 surface and subsequently exposing the surface to oxygen

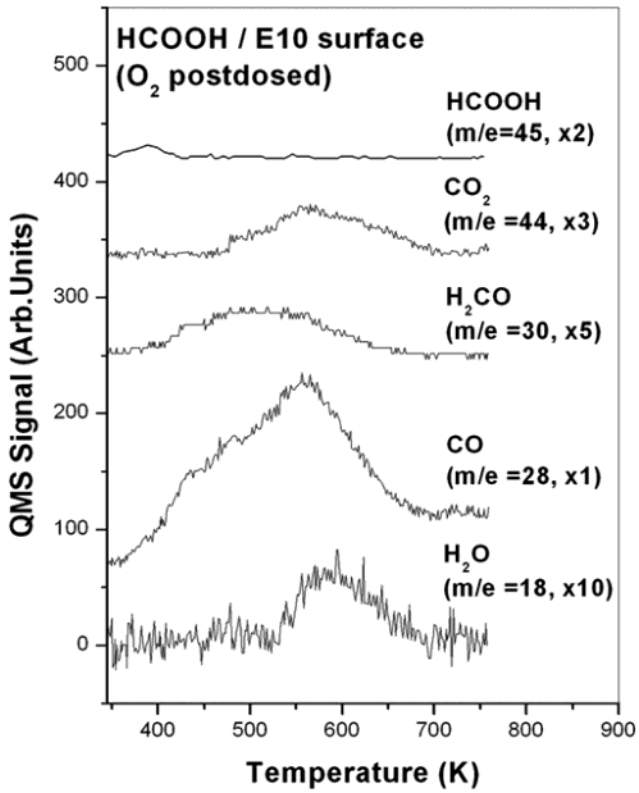

Figure 15. TPR spectra for a saturation exposure of HCOOH on the E10 TiO_2 (110) surface after 120 L of oxygen post-dosed at room temperature. The signals are corrected for QMS sensitivity.

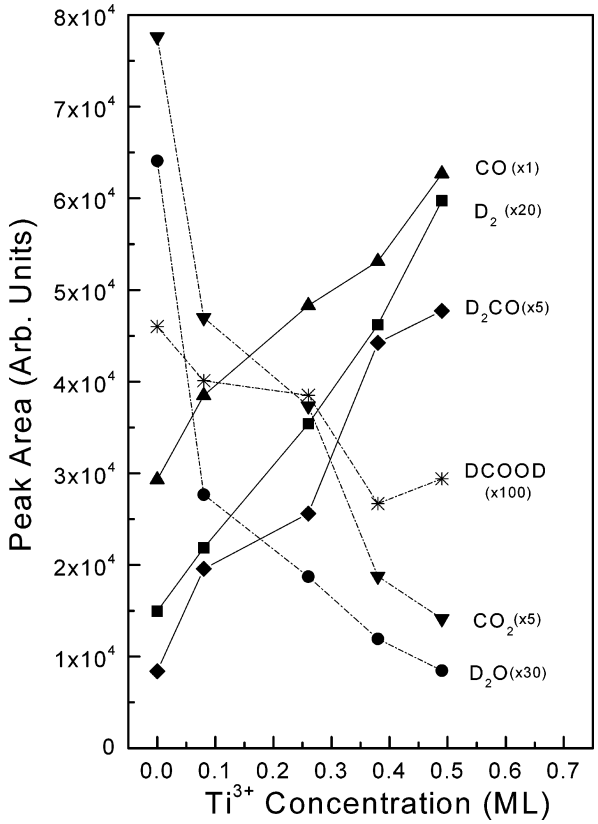

Figure 16. Integrated peak area of D_2 (■), D_2O (high-temperature peak, ●), CO (▲), D_2CO (◆), CO_2 (▼), DCOOD (*) from TPRS of DCOOD versus the defect concentration on the TiO_2 (110) surfaces after electron irradiation.

at room temperature. The TPRS spectra for such an experiment is shown in Figure 15. Several differences were observed between this spectra and the one obtained from the E10 surface in the absence of oxygen. On the oxygen post-dosed surface, CO desorption occurred in two states as it did on the defective surfaces when oxygen was not post-dosed. However, the low temperature peak, which was characteristic of the defective surfaces and dominated on the E10 surface, decreased substantially in favor of the high-temperature peak when oxygen was post-dosed. The area of the low-temperature peak was calculated to be 26% of the total, as opposed to the 66% obtained for the E10 surface in the absence of oxygen. This behavior suggests that oxygen has refilled some of the defects, and that these defects were indeed responsible for the low-temperature CO desorption state. Also, the H_2CO desorption peak decreased by 35% on the oxygen post-dosed surface and shifted back to higher temperature (505 K). This is also consistent with the fact that oxygen is refilling the vacancies since, as shown previously, the H_2CO peak progressively increases in area and shifts to lower temperatures with increasing number of defects. No new products were detected in these experiments that could be attributed to the reaction of formic acid with oxygen. In addition, when $^{18}O_2$ was used for the post-dosing experiment, $^{18}O_2$ was not incorporated into the products, suggesting that the main role of oxygen is to refill vacancies and not to react with the adsorbed species.

IV. Discussion

In summary, the defects created by electron irradiation significantly reduce the temperature for the evolution of CO and formaldehyde. A low-temperature reaction channel grows in importance with increasing defect density, ultimately dominating product formation. The amounts of the reduced products formed (D_2, CO, and formaldehyde) from DCOOD decomposition increase with defect density, while CO_2 formation is suppressed by the defects. This effect is clearly shown in Figure 16, which relates the peak areas for the different products to the defect density.

On the stoichiometric surface the majority of the CO is believed to be the product of unimolecular decomposition of adsorbed formate:[37,38]

$$DCOO^-_{(a)} \rightarrow CO_{(g)} + OD^-_{(a)} \qquad (3)$$

This mechanism is consistent with the observation by STM that formate is formed on the TiO_2 (110) surface and that basic oxygen anions are adjacent to the coordinatively unsaturated Ti^{4+} cations to which formate binds. However, a study by Henderson[38] shows that surface oxygen is exchanged readily into the CO product, and reaction 3 does not account for this occurrence. According to Henderson, "oxygen atoms in adsorbed formate species readily scrambled with lattice oxygen atoms in the TiO_2 (110) surface." The exchanged oxygen appears in CO and formaldehyde in a significant amount above 400 K, at which temperature oxygen vacancies are introduced onto the surface by condensation of bridging hydroxyl groups. This active role of the surface in the reaction has been demonstrated in an STM study by Bowker et al.[9] that showed the formation of a "$(1 \times 1/2)$" structure in islands at the temperature of formate decomposition. This structure was shown to correspond to a (1×1) structure in which several bridging oxygen atoms had been removed.

The exchange of surface oxygen into formate and, subsequently, formaldehyde and CO is consistent with interconversion

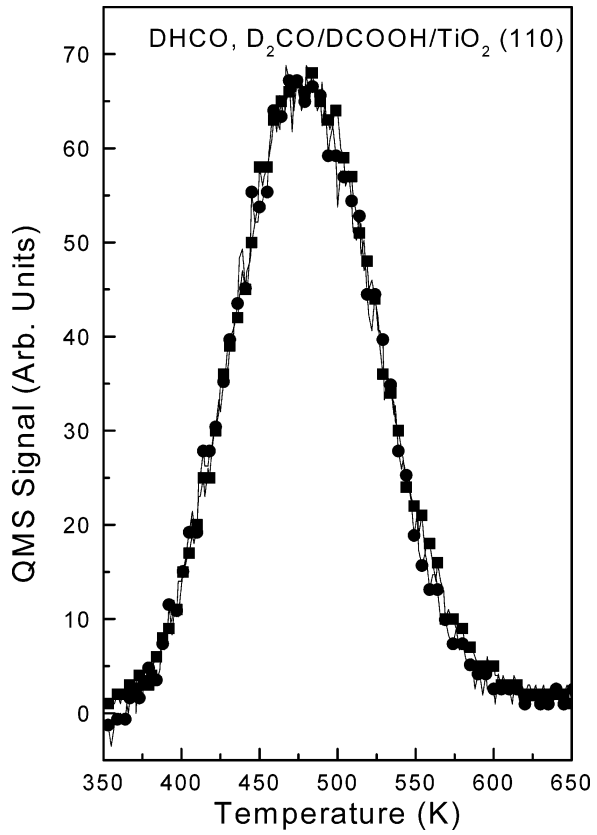

Figure 17. D_2CO (■) and DHCO (●) TPRS spectra from DCOOH decomposition on TiO_2 (110) surface irradiated by electron for 15 min. (DHCO signal was multiplied by 1.6.)

between formate and formyl on this surface, according to

$$DCOO_{(a)} + O_V \rightleftharpoons DCO_{(a)} + O_{(lattice)} \quad (4)$$

where O_V designates an oxygen anion vacancy. The oxygen anion defects serve as sites for the oxygen to be released from the formate anion. Formyl may further decompose to CO or extract a hydrogen atom from a hydroxyl group to form formaldehyde. With increasing defect concentration more formyl is formed, more reoxidation of the surface by formate occurs, and more CO and formaldehyde are formed.

The formyl intermediate has been proposed to participate in many reactions, e.g., reactions between CO and H_2 on rhodium catalysts,[47] decomposition of formic acid on nickel surfaces,[48] and the adsorption of CO on hydrogen-reduced cerium oxide,[49] among others. Its existence on other surfaces has been suggested.[49,50] Its formation on the TiO_2 (110) surface is further supported indirectly from the decomposition of DCOOH on the E15 surface. Shown in Figure 17 is the TPR spectra of D_2CO ($m/e = 32$) and DHCO ($m/e = 31$) from DCOOH decomposition. D_2CO and DHCO were formed in a ratio of 3:2; when scaled, the two spectra track each other very well, indicative of a common rate-limiting reaction intermediate in their formation. The intermediate is very likely to be formyl. D_2CO is formed from the combination of DCO with OD, the decomposition product of DCOO, and DHCO is formed from combination of DCO and residual OH, which results from the dissociation of DCOOH during adsorption and would otherwise disproportionate to form water at about 525 K. Greater intensity of D_2CO than DHCO is reasonable, as most of the OH which resulted from the dissociative adsorption of DCOOH is channeled into H_2O formation at ~410 K (Figure 8). The formyl concentration on the defective surfaces at room temperature is apparently small, as only a single C(1s) peak (289.0 eV), assignable to formate, was detected in the XP spectrum. Assuming the C1s binding energy of formyl is no greater than that of formaldehyde, an additional peak about 1 eV below that of formate[51,52] should be observed if the concentration of formyl is significant. The isotopic effect observed for carbon monoxide formation suggests that C−H bond scission, not the C−O bond breakup, is the rate-limiting step in the formation of carbon monoxide on both the stoichiometric and the electron-irradiated surfaces.

Clearly D_2CO can only be a product of DCOO reduction. Therefore, the amount of D_2CO formed is expected to increase as the number of point defects grows. As shown in Figure 17, no isotopic effect was observed for D_2CO and DHCO production from the decomposition of DCOOH on the E15 surface. This indicates that the rate of formation of formaldehyde on the E15 surface is not limited by the rate of transfer of hydrogen to formyl. The slowest reaction in this process is probably the formation of formyl, though the reaction of formyl with hydroxyl is also a possible rate-limiting step, as no isotopic effect was detected for the liberation of water from this surface either. When the number of defects was decreased by post-dosing oxygen on the defective surfaces, the amount of formaldehyde produced was smaller, supporting the idea that point defects are responsible for the increase in formaldehyde production observed on the defective surfaces. Similarly, the lower-temperature CO peak that had developed in the presence of defects was seen to decrease in the oxygen post-dosing experiments as well, suggesting that oxygen post-dosing did in fact result in filling of anion defects. The filling of anion vacancy defects by exposure to O_2 has been previously reported in the literature.[6,53] Diebold has suggested that the oxygen released in formaldehyde formation may not only be used to fill vacancies but also could react with Ti^{3+} interstitials.[8] An STM study by Bennett et al. on the adsorption of formic acid on the cross-linked (1×2) reconstructed surface has shown that oxygen atoms are inserted into the surface from formate during decomposition, resulting in the formation of new TiO_2 (1×1) islands.[10]

In addition to the oxidation state of the titanium, surface structure also plays an important role in determining the selectivity of the decomposition of the acid to formaldehyde. The selectivity of the reaction for formaldehyde on the Ar^+-bombarded surface is lower than that on the E15 surface, which has a similar defect concentration. Further, the peak temperature on the two surfaces is dramatically different, being significantly lower on the electron-irradiated surface. A dependence of the selectivity to formaldehyde on the surface structure was also noticed on the TiO_2 (001) surface by Idriss et al.[29] They observed that the yield of formaldehyde from formic acid decomposition first decreased and then increased with the annealing temperature of the Ar^+-bombarded TiO_2 (001) surface.

The effect of defects created by Ar^+ bombardment on the TiO_2 (110) surface on the steady-state decomposition of formic acid has been previously investigated.[54] No difference in the catalytic activity of the Ar^+-bombarded partially annealed and the well-ordered TiO_2 (110) surfaces for the DCOOD decomposition was detected. Our TPRS results confirm the finding of Onishi et al. that the activity of DCOOD decomposition to CO was not altered by Ar^+ bombardment, as the temperature at which CO evolved from both the stoichiometric and the Ar1 surfaces is the same. However, our results show a significant drop in selectivity to CO_2 after Ar^+ bombardment. That they did not see a change in the production of CO_2 is probably due to reoxidation of the ion-bombarded surface during the exposure

to formic acid required to reach steady state at the elevated temperatures of the experiments; the reactivity detected may no longer reflect the defective state of the original reduced surface.

The low-temperature peak for water desorption from the stoichiometric surface is believed to originate from the recombination of hydroxyl groups on the surface, which have been formed from formic acid dissociation during adsorption:[38]

$$DCOOD + O^{2-}_{(lattice)} \rightarrow DCOO^{-}_{(a)} + OD^{-}_{(lattice)} \quad (1)$$

$$2OD^{-}_{(lattice)} \rightarrow D_2O_{(g)} + O^{2-}_{(lattice)} + O_v \quad (2)$$

where "O_v" refers to an oxygen vacancy site, "a" denotes an adsorbed species and "g" a gaseous species. It is reasonable to assume that the lower temperature water peak on the defective surfaces has the same origin. It appears that the reactivity of water formation from hydroxyl groups at this low temperature channel is not significantly affected by the presence of point defects. Lu and co-workers[19] also observed that water desorbed at the same temperature on stoichiometric and defective TiO_2 (110) surfaces. The decrease in the magnitude of the high-temperature water peak with the electron irradiation time is consistent with observations that (1) the oxygen from the adsorbed formate is retained by the surface to reoxidize the Ti^{3+} cations, and (2) hydrogen from formic acid is diverted to dihydrogen and formaldehyde, as the amounts of both products formed show significant increase on the defective surfaces.

Regarding the minor products, several reactions have been proposed for the production of CO_2 from formate on TiO_2 (110) surfaces, including:[7,37,38]

$$OD^{-}_{(a)} + DCOO^{-}_{(a)} \rightarrow D_{2(g)} + CO_{2(g)} + O^{2-}_{(a)} \quad (5)$$

$$DCOO^{-}_{(a)} + DCOOD_{(g)} \rightarrow CO_{2(g)} + D_{2(g)} + DCOO^{-}_{(a)} \quad (6)$$

$$2DCOO^{-}_{(a)} + O_v \rightarrow CO_2 + D_2CO + O^{2-}_{(lattice)} \quad (7)$$

Reactions 5 and 6 were proposed in accord with the assumption that equivalent amount of D_2 and CO_2 should be produced from DCOOD decomposition on the TiO_2 (110) surface. However, experimental results show this assumption to be incorrect, as the amount of CO_2 exceeds that of D_2 produced on the stoichiometric surface. But this fact alone does not rule out the existence of reactions 5 and 6. Reaction 7 is not likely to occur, at least as an elementary step, as the CO_2 and D_2CO desorption peaks are not concomitant, and the introduction of oxygen vacancies suppresses CO_2 production.

Other reaction channels could exist, e.g.:

$$O_{(lattice)} + DCOO_{(a)} \rightarrow OD_{(a)} + CO_{2(g)} \quad (8)$$

$$DCOO_{(a)} \rightarrow D_{(a)} + CO_{2(g)} \quad (9)$$

$$OD_{(a)} + DCOO_{(a)} \rightarrow D_2O_{(g)} + CO_{2(g)} \quad (10)$$

The inclusion of these reactions can account for the inequivalence of D_2 and CO_2 in the decomposition products. CO_2 desorbs in two temperature ranges on all the surfaces studied. The two desorption peaks may originate from two different reactions or one reaction which proceeds under different local conditions. It is hard to distinguish these two cases from the present experiments, as the reaction mechanisms involved are still unclear. Iwasawa et al.[11,12] have reported a different adsorbate on the bridging oxygen rows which was observed by STM during reaction and have identified it as a carbonate species (CO_3^{2-}). This species may be responsible for some of the CO_2 production. The suppression of the production of CO_2 by defects could be because Ti^{3+} has a higher affinity for oxygen atoms than the 5-fold coordinated Ti^{4+}, and the oxygen in formate is prone to extraction by Ti^{3+}.

Clearly the increase in the amount of D_2 formed with increasing Ti^{3+} concentration indicates that the anion defects promote D_2 formation. Chemisorption of H_2 on defective TiO_2 (110) surfaces produced by high-temperature annealing has been reported, and it was suggested that H_2 dissociates to form $Ti^{4+}-H^-$ bonds during the process.[32,55,56] Recently, bright features on a STM image of a TiO_2 (110) surface annealed at 900 K were assigned to Ti−H species.[57] On defective surfaces the D atom may be extracted from $DCOO^-$/DCO by Ti^{3+} sites on the surface to form $Ti^{4+}-D^-$ pairs; the D atoms then combine to form D_2. D_2 also could be the product of the condensation of the hydroxyl groups on the surface generated during DCOOD dissociative adsorption, as observed by Lu and co-workers.[19] The existence of the second channel is supported by the production of H_2 from DCOOH decomposition on both stoichiometric and E15 surfaces. In either case, higher defect concentrations on the surface should produce larger amounts of D_2, as observed. The complete decomposition of formate to yield D, C, and lattice oxygen is unlikely, as no residual carbon was detected by XPS.

The defects generated by electron irradiation are different from those generated by Ar^+ bombardment in several ways. First, the TPR spectra for DCOOD decomposition on the surfaces with similar defect concentration are quite different. Second, their reoxidizability by formic acid differs significantly. The differences may result from the local structure around the Ti^{3+} cations. On the surfaces irradiated by electron beam, the defects are believed to be created by removing the bridging oxygen on the surface, at least at low defect concentration. The surface structure may exhibit little rearrangement, the defects assuming a distorted pyramidal coordination structure. On the Ar^+-bombarded surface, there is significant surface reconstruction, and the surface is believed to be similar to that of Ti_2O_3,[58] which has the structure of corundum with Ti^{3+} in an octahedral coordination.

V. Summary

When oxygen anion defects are introduced into the stoichiometric TiO_2 (110) surface by electron-beam irradiation in different concentration, new active sites for DCOOD reduction to CO and formaldehyde are generated which lower the activation energy and increase the selectivity for the reaction products. The pattern of reactivity is strongly suggestive of the participation of formyl as the rate-limiting reactive intermediate. Ti^{3+} defects introduced by Ar^+ bombardment show a very different reactivity at the same defect concentration, suggesting significant differences in the nature of the active sites on the defective surfaces generated by the different methods.

Acknowledgment. The authors gratefully acknowledge the support of the National Science Foundation through NSF CTS 0000283.

References and Notes

(1) Chung, Y. W.; Lo, W. J.; Somorjai, G. A. *Surf. Sci.* **1977**, *64*, 588.
(2) Rohrer, G. S.; Henrich, V. E.; Bonnell, D. A. *Surf. Sci.* **1992**, *278*, 146.
(3) Onishi, H.; Fukui, K.; Iwasawa, Y. *Bull. Chem. Soc. Jpn.* **1995**, *68*, 2447.

(4) Diebold, U.; Lehman, J.; Mahmound, T.; Kuhn, M.; Leonardelli, G.; Hebenstreit, W.; Schmid, M.; Varga, P. *Surf. Sci.* **1998**, *411*, 137.
(5) Bennett, R. A.; Stone, P.; Price, N. J.; Bowker, M. *Phys. Rev. Lett.* **1999**, *82*, 3831.
(6) Epling, W. S.; Peden, C. H. F.; Henderson, M. A.; Diebold, U. *Surf. Sci.* **1998**, *412/413*, 333.
(7) Sherrill, A. B.; Barteau, M. A. Principles of Reactivity from Studies of Organic Reactions on Model Oxide Surfaces. In *Oxide Surfaces*, 1st ed.; Woodruff, D. P., Ed.; Elsevier Science B. V.: Amsterdam, 2001; Vol. 9, p 409.
(8) Diebold, U. *Surf. Sci. Rep.* **2003**, *48*, 53.
(9) Bowker, M.; Stone, P.; Bennett, R.; Perkins, N. *Surf. Sci.* **2002**, *511*, 435.
(10) Bennett, R. A.; Stone, P.; Smith, R. D.; Bowker, M. *Surf. Sci.* **2000**, *456*−*456*, 390.
(11) Iwasawa, Y.; Onishi, H.; Fukui, K.; Suzuki, S.; Sasaki, T. *Faraday Discuss.* **2000**, *114*, 259.
(12) Iwasawa, Y.; Onishi, H.; Fukui, K. *Top. Catal.* **2001**, *14*, 163.
(13) Sasahara, A.; Uetsuka, H.; Onishi, H. *J. Phys. Chem. B* **2001**, *105*, 1.
(14) Gutiérrez-Sosa, A.; Martínez-Escolano, P.; Raza, H.; Lindsay, R.; Wincott, P. L.; Thornton, G. *Surf. Sci.* **2001**, *471*, 163.
(15) Chang, Z.; Thornton, G. *Surf. Sci.* **2000**, *462*, 68.
(16) Käckell, P.; Terakura, K. *Appl. Surf. Sci.* **2000**, *166*, 370.
(17) Käckell, P.; Terakura, K. *Surf. Sci.* **2000**, *461*, 191.
(18) Henrich, V. E.; Cox, P. A. *The Surface Science of Metal Oxides*; Cambridge University Press: Cambridge, 1994.
(19) Lu, G.; Linsebigler, A.; Yates, J. T., Jr. *J. Phys. Chem.* **1994**, *98*, 11733.
(20) Wang, L.; Baer, D. R.; Engelhard, M. H. *Surf. Sci.* **1994**, *320*, 295.
(21) Pétigny, S.; Mostéfa-Sba, H.; Domenichini, A.; Lenieswska, E.; Steinbrunn, A.; Bourgeouis, S. *Surf. Sci.* **1998**, *410*, 250.
(22) Pétigny, S.; Domenichini, A.; Mostéfa-Sba, H.; Lenieswska, E.; Steinbrunn, A.; Bourgeouis, S. *Appl. Surf. Sci.* **1999**, *142*, 114.
(23) Pan, J. M.; Maschhoff, B. L.; Diebold, U.; Madey, T. E. *J. Vac. Sci. Technol. A* **1992**, *10*, 2470.
(24) Wang, L. Q.; Ferris, K. F.; Shultz, A. N.; Baer, D. R.; Engelhard, M. H. *Surf. Sci.* **1997**, *380*, 352.
(25) Eriksen, S.; Egdell, R. G. *Surf. Sci.* **1987**, *180*, 263.
(26) Kim, K. S.; Barteau, M. A. *J. Catal.* **1990**, *125*, 353.
(27) Murray, P. W.; Condon, N. G.; Thornton, G. *Phys. Rev. B* **1995**, *51*, 10989.
(28) Cocks, I. D.; Guo, Q.; Williams, E. M. *Surf. Sci.* **1997**, *390*, 119.
(29) Idriss, H.; Lusvardi, V. S.; Barteau, M. A. *Surf. Sci.* **1996**, *348*, 39.
(30) Wang, L.-Q.; Ferris, K. F.; Skiba, P. X.; Shultz, A. N.; Baer, D. R.; Engelhard, M. H. *Surf. Sci.* **1999**, *440*, 60.
(31) Linsebigler, A.; Lu, G.; Yates, J. T., Jr. *J. Chem. Phys.* **1995**, *103*, 9438.
(32) Göpel, W.; Rocker, G.; Feierabend, R. *Phys. Rev. B* **1983**, *28*, 3427.
(33) Muryn, C. A.; Hardman, P.; Crouch, J. J.; Raiker, G. N.; Thornton, G.; Law, S. D.-L. *Surf. Sci.* **1991**, *251/252*, 747.
(34) Wang, L.-Q.; Baer, D. R.; Engelhard, M. H.; Shultz, A. N. *Surf. Sci.* **1995**, *344*, 237.
(35) Kim, K. S.; Barteau, M. A. *Langmuir* **1990**, *6*, 1485.
(36) Farfan-Arribas, E.; Madix, R. J. *J. Phys. Chem. B* **2002**, *106*, 10680.
(37) Onishi, H.; Aruga, T.; Iwasawa, Y. *J. Catal.* **1994**, *146*, 557.
(38) Henderson, M. A. *J. Phys. Chem. B* **1997**, *101*, 221.
(39) Sambi, M.; Sangiovanni, G.; Graznozzi, G.; Parmigiani, F. *Phys. Rev. B* **1997**, *55*, 7850.
(40) Price, N. J.; Reitz, J. B.; Madix, R. J.; Solomon, E. I. *J. Electron Spectrosc. Relat. Phenom.* **1999**, *98/99*, 257.
(41) Göpel, W.; Anderson, J. A.; Frankel, D.; Jaehnig, M.; Phillips, K.; Schäfer, J. A.; Rocker, G. *Surf. Sci.* **1984**, *139*, 333.
(42) Thevuthasan, S.; Herman, G. S.; Kim, Y. J.; Chambers, S. A.; Peden, C. H. F.; Wang, Z.; Ynzunza, R. X.; Tober, E. D.; Morais, J.; Fadley, C. S. *Surf. Sci.* **1998**, *401*, 261.
(43) Chambers, S. A.; Henderson, M. A.; Kim, Y. J.; Thevuthasan, S. *Surf. Rev. Lett.* **1998**, *5*, 381.
(44) Iwasawa, Y. *Surf. Sci.* **1998**, *402*−*404*, 8.
(45) Hayden, B. E.; King, A.; Newton, M. A. *J. Phys. Chem. B* **1999**, *103*, 203.
(46) Henderson, M. A. *J. Phys. Chem.* **1995**, *99*, 15253.
(47) Breault, R.; Hindermann, J. P.; Kiennemann, A.; Laurin, M. *Stud. Surf. Sci. Catal.* **1984**, *19*, 489.
(48) Raupp, G. B.; Dumesic, J. A. *J. Phys. Chem.* **1986**, *90*, 3359.
(49) Li, C.; Sakata, Y.; Arai, T.; Domen, K.; Maruya, K.; Onishi, T. *J. Chem. Soc., Faraday Trans. 1* **1989**, *85*, 1451.
(50) Mitchell, W. J.; Wang, Y.; Xie, J.; Weinberg, W. H. *J. Am. Chem. Soc.* **1993**, *115*, 4381.
(51) Vohs, J. M.; Barteau, M. A. *Surf. Sci.* **1986**, *176*, 91.
(52) Idriss, H.; Kim, K. S.; Barteau, M. A. *Surf. Sci.* **1992**, *262*, 113.
(53) Henderson, M. A.; Epling, W. S.; Perkins, C. L.; Peden, C. H. F.; Diebold, U. *J. Phys. Chem. B* **1999**, *103*, 5328.
(54) Yamaguchi, Y.; Onishi, H.; Iwasawa, Y. *J. Chem. Soc., Faraday Trans.* **1995**, *91*, 1663.
(55) Knotek, M. L. *Surf. Sci. Lett.* **1980**, *91*, 17.
(56) Knotek, M. L. *Surf. Sci.* **1980**, *101*, 334.
(57) Suzuki, S.; Fukui, K.; Onishi, H.; Iwasawa, Y. *Phys. Rev. Lett.* **2000**, *84*, 2156.
(58) Henrich, V. E.; Dresselhaus, G.; Zeiger, H. J. *Phys. Rev. Lett.* **1976**, *36*, 1335.